Metabolic shifts in residual breast cancer drive tumor recurrence

Kristina M. Havas,[1,2] Vladislava Milchevskaya,[3] Ksenija Radic,[3] Ashna Alladin,[3] Eleni Kafkia,[3] Marta Garcia,[3] Jens Stolte,[1] Bernd Klaus,[3] Nicole Rotmensz,[4] Toby J. Gibson,[3] Barbara Burwinkel,[5] Andreas Schneeweiss,[6] Giancarlo Pruneri,[7] Kiran R. Patil,[3] Rocio Sotillo,[1,8,9] and Martin Jechlinger[1,3]

[1]EMBL Monterotondo, Adriano Buzzati-Traverso Campus, Monterotondo, Italy. [2]Istituto Firc di Oncologia Molecolare (IFOM) the Italian Foundation for Cancer Research (FIRC) Institute of Molecular Oncology, Milan, Italy. [3]EMBL Heidelberg, Heidelberg, Germany. [4]Division of Epidemiology and Biostatistics European Institute of Oncology, Milan, Italy. [5]Molecular Biology of Breast Cancer, University Women's Clinic, Heidelberg, Germany. [6]Gynecologic Oncology, National Center for Tumor Diseases, University of Heidelberg, Heidelberg, Germany. [7]Department of Pathology, Biobank for Translational Medicine Unit, European Institute of Oncology, Milan and University of Milan, School of Medicine, Milan, Italy. [8]Division of Molecular Thoracic Oncology, German Cancer Research Center (DKFZ), Heidelberg, Germany. [9]Translational Lung Research Center Heidelberg (TLRC), German Center for Lung Research (DZL), Heidelberg, Germany.

Tumor recurrence is the leading cause of breast cancer–related death. Recurrences are largely driven by cancer cells that survive therapeutic intervention. This poorly understood population is referred to as minimal residual disease. Here, using mouse models that faithfully recapitulate human disease together with organoid cultures, we have demonstrated that residual cells acquire a transcriptionally distinct state from normal epithelium and primary tumors. Gene expression changes and functional characterization revealed altered lipid metabolism and elevated ROS as hallmarks of the cells that survive tumor regression. These residual cells exhibited increased oxidative DNA damage, potentiating the acquisition of somatic mutations during hormonal-induced expansion of the mammary cell population. Inhibition of either cellular fatty acid synthesis or fatty acid transport into mitochondria reduced cellular ROS levels and DNA damage, linking these features to lipid metabolism. Direct perturbation of these hallmarks in vivo, either by scavenging ROS or by halting the cyclic mammary cell population expansion, attenuated tumor recurrence. Finally, these observations were mirrored in transcriptomic and histological signatures of residual cancer cells from neoadjuvant-treated breast cancer patients. These results highlight the potential of lipid metabolism and ROS as therapeutic targets for reducing tumor recurrence in breast cancer patients.

Introduction

Despite advances in detection and therapy, breast cancer remains the second leading cause of cancer-related death in women. Mortality is largely due to tumor recurrence following initial therapeutic intervention (1). Recurrence arises from local and/or disseminated residual cancer cells, which survive treatment and are generally referred to as minimal residual disease (MRD) (2). The concept of MRD as the substrate for tumor recurrence is strongly supported by the negative prognostic value associated with the persistence of disseminated tumor cells in breast cancer patients following neoadjuvant therapies (3). Despite its central role in breast cancer progression, in-depth characterization of this population has been hindered by the difficulty in obtaining clinical samples of MRD.

Due to the elusive nature of MRD in patients, animal models that faithfully recapitulate human disease and permit the study of MRD are the method of choice to understand mechanisms of recurrence (4). Here, we utilize 2 conditional mouse models of recurrent mammary tumorigenesis; *TetO-cMYC TetO-Neu MMTV-rtTA* (hereafter referred to as MYC/NEU) and *TetO-cMYC TetO-Kras^{G12D} MMTV-rtTA* (hereafter referred to as MYC/KRAS) (5–7). In both models, tissue-specific induction of oncogene expression results in the rapid onset of invasive mammary carcinomas. These tumors display strong oncogene addiction; hence, following oncogene inactivation, they completely regress to a nonpalpable state (5–7). As in breast cancer patients, these mice develop spontaneous tumor recurrences after complete regression, making them suitable models of MRD (5).

To characterize minimal residual cancer cells, we established organotypic 3-dimensional (3D) cultures of primary mammary epithelial cells (organoids) from our mouse models (8). These models permitted isolation of pure residual cancer cell populations following oncogene inactivation. Transcriptome analysis of residual cells revealed a dormancy signature along with strong alterations in lipid metabolism — features we could verify both in mice and in tissue obtained from human breast cancer patients following successful neoadjuvant therapy. Here, we address the consequence of aberrant lipid metabolism in MRD, demonstrating that altered lipid metabolism coupled with restricted antioxidant capacity drives the accumulation of ROS and DNA adducts, which potentiate tumor recurrence.

Results

Oncogene inactivation results in persistence of a transcriptionally distinct state with defining metabolic signatures. To overcome the covert nature of MRD, we employed organoid cultures of primary

Conflict of interest: The authors have declared that no conflict of interest exists.
Submitted: August 4, 2016; **Accepted:** March 16, 2017.
Reference information: *J Clin Invest*. 2017;127(6):2091–2105.
https://doi.org/10.1172/JCI89914.

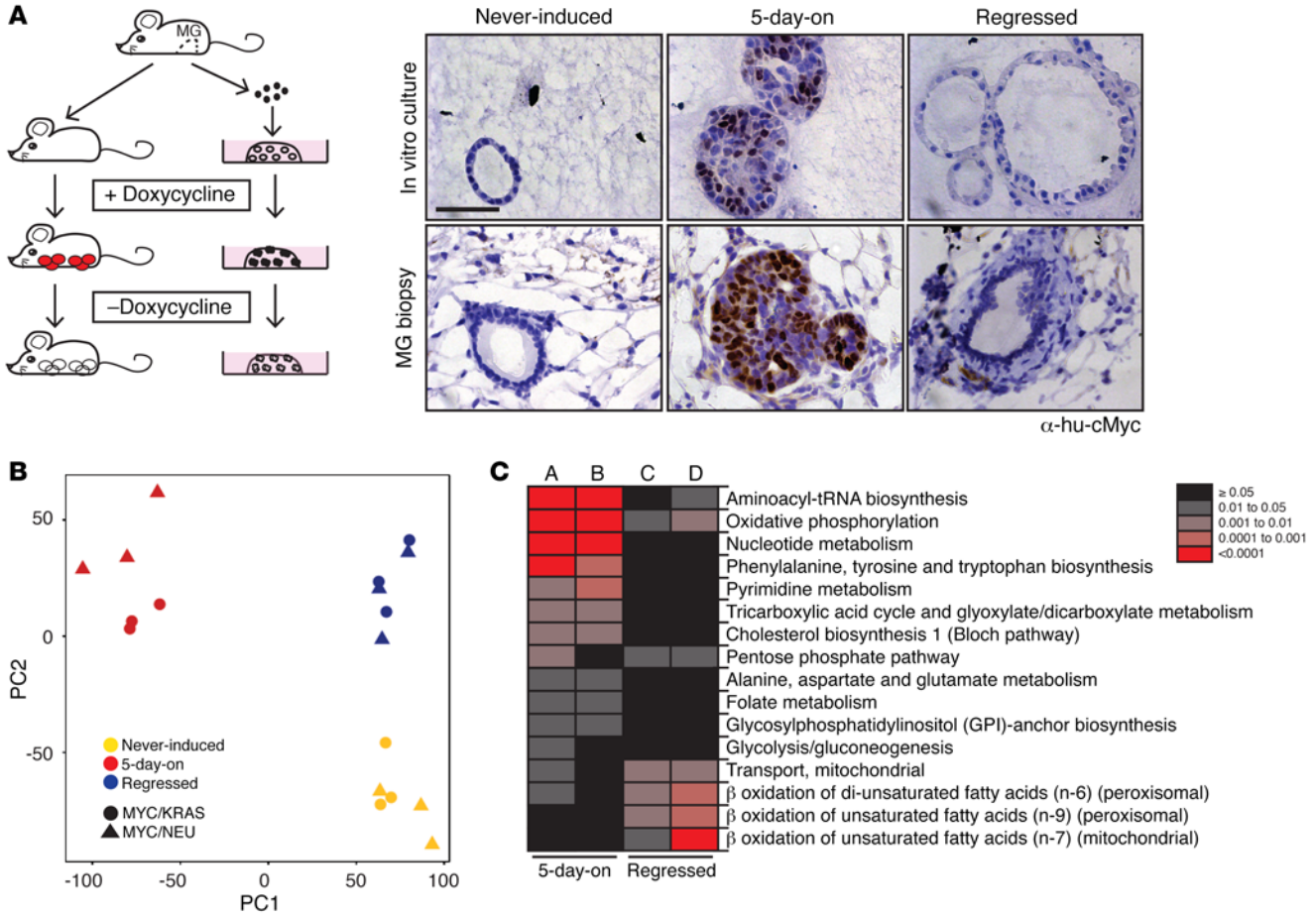

Figure 1. Identifying temporally deregulated genes in a breast cancer model. (**A**) Left panel: Mouse models of recurrent mammary tumorigenesis were used for in vivo studies. These studies were complemented by organoid cultures derived from primary mammary epithelial cells isolated from adult (>8 weeks of age), virgin mice. MG, mammary gland. Red circles, mammary tumors; white circles, regressed tissue; black-filled dots, in vitro tumor correlates; hollow dots, in vitro regressed tissue correlates. Right panel: in vitro (right upper panels) and corresponding in vivo (right lower panels) transgene-specific c-Myc staining of acini/mammary glands at the never-induced, 5-day-on, and regressed (5 days in the presence of doxycycline, then 7 days grown in media without doxycycline) timepoints. Scale bar: 50 μm. (**B**) Principal component analysis of variance-stabilization and normalization–processed (VSN-processed) expression data from never-induced (yellow), 5-day-on doxycycline (red), and regressed (blue) MYC/KRAS and MYC/NEU cultures. (**C**) Reporter pathways upregulated in gene sets derived from the comparisons of never-induced to tumor correlate (5-day-on) and never-induced to MRD correlate (regressed) in both MYC/KRAS and MYC/NEU cultures. A, MYC/NEU 5-day-on versus never-induced; B, MYC/KRAS 5-day-on versus never-induced; C, MYC/NEU regressed versus never-induced; and D, MYC/KRAS regressed versus never-induced.

mammary epithelial cells for transcriptional characterization of this rare population (8). Cells were derived from preclinical mouse models of recurrent breast cancer in which the tissue-specific expression of MYC/KRAS or MYC/NEU (NEU is also known as HER2) were regulated by doxycycline (Figure 1A). Briefly, primary mammary epithelial cells were isolated from adult (>8 weeks of age) virgin mice, and a single cell suspension was seeded into Matrigel, where the cells developed into hollow, polarized acinar structures. Doxycycline addition to the media induced transgene expression, resulting in a rapid onset of proliferation and filling of the acini. Following 5 days of induction, the doxycycline was removed from the media. Strong oncogene addiction in these models resulted in a rapid onset of apoptosis upon oncogene silencing by doxycycline removal (Supplemental Figure 1A; supplemental material available online with this article; https://doi.org/10.1172/JCI89914DS1). The population of cells that survive oncogene withdrawal are referred to as regressed and represent an MRD correlate state. Use of this system allowed us to isolate synchronized cultures that closely mirrored the histological changes and expression kinetics observed in mammary gland biopsies spanning from steady state to tumor induction through to a regressed (MRD correlate) state (Figure 1A and Supplemental Figure 1, A and B; ref. 8).

The cellular homogeneity and high degree of synchronicity of the organoid culture system allowed us to identify pure transcriptional profiles of cells surviving oncogene inactivation. We performed gene expression profiling of 3 stages of the organoid cultures: cells that had never expressed the oncogenes (never-induced), cells that had expressed both oncogenes for 5 days (5-day-on), and cells that had undergone a cycle of oncogene expression for 5 days and subsequent deinduction for 7 days (regressed). Expression data were normalized using the robust multiarray average technique in the Oligo package, and they were adjusted for batch effects using the variance stabilization and normalization, and surrogate vari-

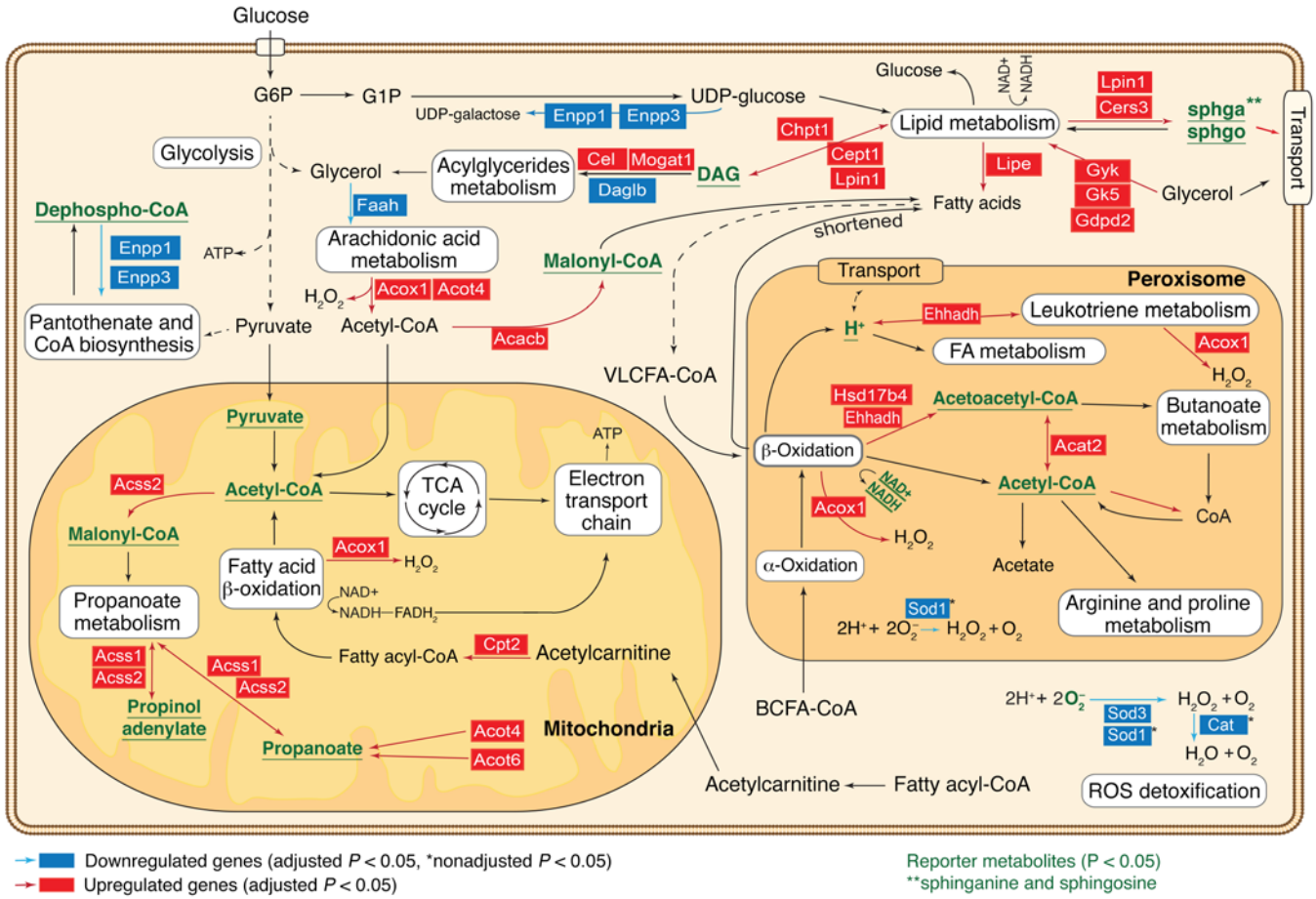

Figure 2. Reporter metabolite analysis reveals key metabolic nodes dysregulated in the regressed population. Overview of metabolic pathways, which become transcriptionally deregulated following MYC/NEU and MYC/KRAS inactivation in comparison with the never-induced control cells. Key metabolic reactions and pathways associated with reporter metabolites (Supplemental Methods/MIAME section) are shown. Reporter metabolites with nonadjusted $P \leq 0.05$, which are predicted to be deregulated in both oncogenic perturbations, are marked in green, while deregulated genes common to both datasets are highlighted.

able analysis packages ($n = 1$ surrogate variables) in Bioconducter (9, 10). Principal component analysis (PCA) of the gene expression profiles revealed overlapping time point–dependent clustering for MYC/KRAS and MYC/NEU transcriptional profiles (Figure 1B). In addition to a clear separation from the 5-day-on state, we identified distinct transcriptional differences between the never-induced and regressed populations (Figure 1B). This was unanticipated, given the phenotypic similarity (Figure 1A) and the absence of oncogenic signals in both states (Supplemental Figure 1B).

Several Gene Set Enrichment Analysis (GSEA) tools were employed for the initial characterization of the differentially regulated gene sets associated with the regressed state. These analyses indicated that regressed cells were largely a dormant population, due to the underrepresentation of several pathways associated with cell cycle progression. This is in line with our observations of very low Ki-67 positivity in residual acini following regression (Supplemental Figure 1A). On the other hand, the overrepresented gene sets indicated that the regressed cells, while largely dormant, retained a degree of oncogenic memory and appeared to harbor alterations in cellular metabolism (Supplemental Figure 1, C and D).

Next, we asked if the alterations in cellular metabolism observed in residual cells reflected attributes of the initial tumor metabolism. To tackle this, we performed metabolism-specific pathway enrichment analysis for the differentially expressed genes when comparing the tumor (5-day-on) versus never-induced states, in addition to the regressed versus never-induced states. Significantly enriched metabolic pathways (reporter pathways) were thereby identified as those containing no less than 3 genes in a set and a nonadjusted P value threshold of 0.05. The 5-day-on cultures for both MYC/KRAS and MYC/NEU displayed strong upregulation of multiple pathways, including oxidative phosphorylation, glycolysis, and pentose phosphate pathway, in support of the increased demands for biomass required to sustain growth and proliferation (Figure 1C and Supplemental Table 1). Within the regressed population, we observed persistence of 2 specific pathways found in the tumor state — namely, the oxidative phosphorylation and the pentose phosphate pathways. The analysis also revealed evidence for modulation of lipid catabolic pathways, such as mitochondrial and peroxisomal β-oxidative pathways, suggesting a pronounced alteration in lipid metabolism unique for the regressed state (Figure 1C).

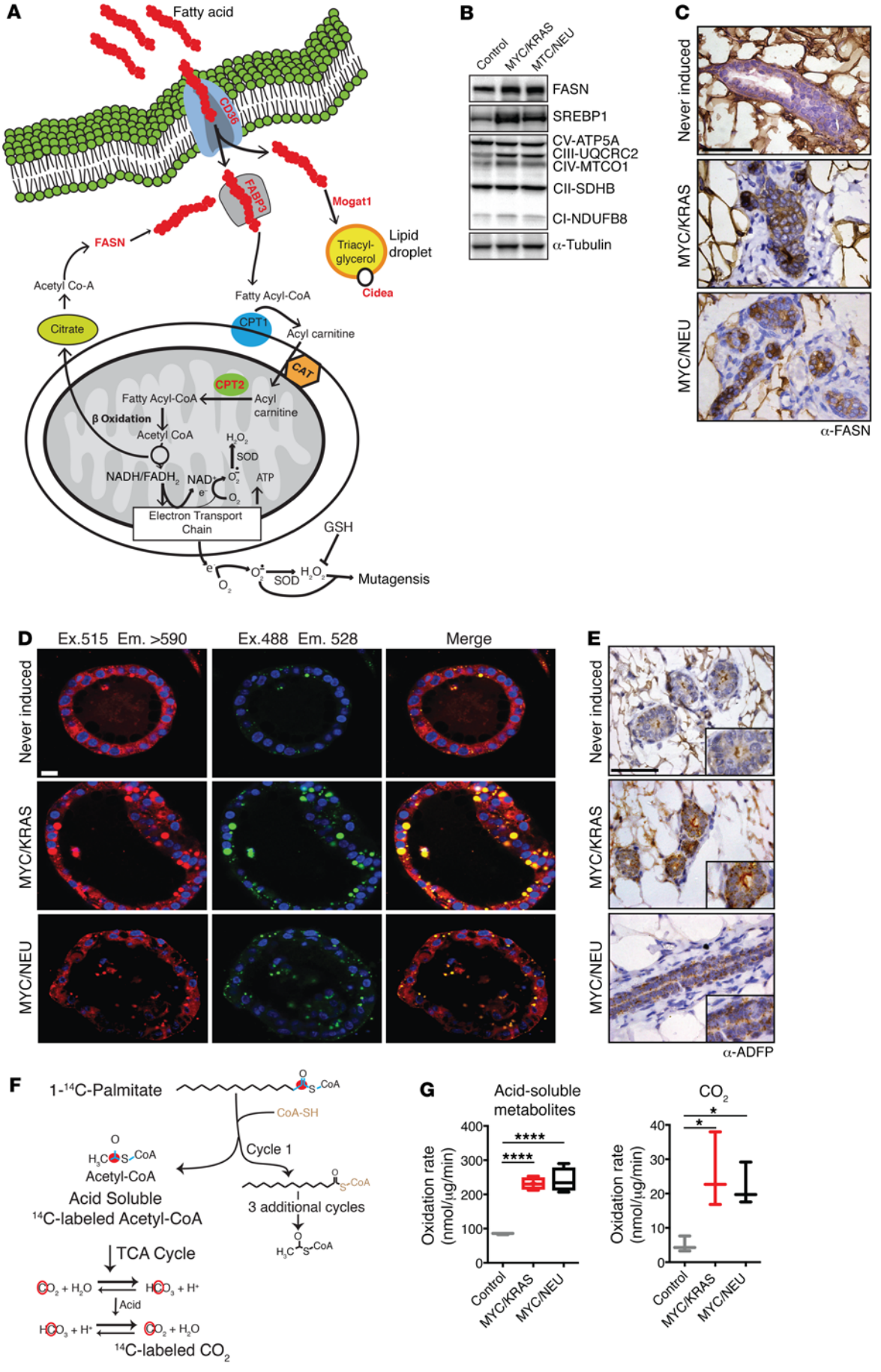
A
Fatty acid
CD36
FABP3
Mogat1
Triacyl-glycerol
Lipid droplet
Cidea
FASN
Acetyl Co-A
Fatty Acyl-CoA
Citrate
CPT1
Acyl carnitine
CAT
CPT2
Fatty Acyl-CoA
Acyl carnitine
β Oxidation
Acetyl CoA
SOD
NADH/FADH2
NAD+
ATP
Electron Transport Chain
GSH
SOD
Mutagensis
B
Control
MYC/KRAS
MTC/NEU
FASN
SREBP1
CV-ATP5A
CIII-UQCRC2
CIV-MTCO1
CII-SDHB
CI-NDUFB8
α-Tubulin
C
Never induced
MYC/KRAS
MYC/NEU
α-FASN
D
Ex.515 Em. >590
Ex.488 Em. 528
Merge
Never induced
MYC/KRAS
MYC/NEU
E
Never induced
MYC/KRAS
MYC/NEU
α-ADFP
F
1-14C-Palmitate
CoA-SH
Cycle 1
Acetyl-CoA
Acid Soluble
14C-labeled Acetyl-CoA
3 additional cycles
TCA Cycle
Acid
14C-labeled CO2
G
Acid-soluble metabolites
Oxidation rate (nmol/μg/min)
Control
MYC/KRAS
MYC/NEU
CO2
Oxidation rate (nmol/μg/min)
Control
MYC/KRAS
MYC/NEU

Figure 3. Increased lipid metabolism as underlining hallmark of the regressed population. (**A**) Schematic illustrating major deregulated lipid metabolism pathways and overexpressed genes (red) in the regressed populations versus the never-induced population. (**B**) Western blots of replicate samples run on multiple gels for several lipid metabolic genes: FASN, SREBP1, and 5 members of the mitochondrial respiratory chain complex (CI-V). Lysates of mammary glands isolated from control, MYC/KRAS, and MYC/NEU regressed mice; replicate samples were run on parallel gels; loading control, α-tubulin. (**C**) IHC of control and regressed mammary glands for FASN. Scale bar: 50 μm. (**D**) Nile red staining of lipid droplets in in vitro–cultured regressed structures from MYC/KRAS and MYC/NEU and never-induced structures. Scale bar: 14 μm. Quantification of lipid droplets was performed for n = 3 MYC/KRAS and MYC/NEU regressed, and n = 4 never-induced structures. Ex., excitation; Em., emission. MYC/KRAS vs. MYC/NEU (P = 0.75), never-induced vs. MYC/KRAS (P = 0.0017), and never-induced vs. MYC/NEU (P = 0.0025); 2 tailed t tests. (**E**) IHC for lipid droplet associated protein adipophilin in regressed mammary glands vs. controls. Scale bar: 50 μm. (**F**) Schematic illustrating assay for mitochondrial palmitate oxidative flux using 1-^{14}C Palmitate (left). 1-^{14}C-Palmitate provides a tractable carbon source for β-oxidative processing, with the read-out being the acid soluble metabolite (ASM) ^{14}C-Acetyl-CoA and ^{14}C-labeled CO_2 produced by the TCA cycle. (**G**) Measurements of ASM and CO_2 produced in mitochondria isolated from age-matched control, MYC/KRAS, and MYC/NEU regressed mice; values are normalized against total protein concentration (right). CO_2 measurements: MYC/KRAS vs. control (P = 0.0235) and MYC/NEU vs. control (P = 0.0489), for ASM measurements: MYC/KRAS vs. control (P < 0.0001) and MYC/NEU vs. control (P < 0.0001). Represented for n = 3 control, n = 4 MYC/KRAS and MYC/NEU biological replicates; one-way ANOVA with Dunnett's multiple comparison test. Data represented as mean ± SEM; *P < 0.05, ****P < 0.0001

To gain a deeper insight into the status of these cells, we mapped the gene expression changes of regressed organoids, in comparison with the never-induced state, onto a genome-scale metabolic network and identified dysregulated metabolic nodes (so-called reporter metabolites) specifically in residual cancer cells (Supplemental Table 2; see Supplemental Methods) (11–13). These metabolites had significant enrichment of transcriptional changes in the genes coding for the corresponding producing or consuming reactions, suggesting altered flux. The identified reporter metabolites confirmed specific derogation of fatty acids (FAs), as well as peroxisomal and mitochondrial lipid metabolic nodes in the cell population that survived oncogene withdrawal. We also observed significant downregulation of peroxisomal and cytoplasmic genes involved in ROS detoxification (Figure 2). The general upregulation of early lipid biosynthesis, FA transport, and FA metabolism, which generates ROS, coupled with a decrease of ROS detoxification enzymes predicts that residual cancer cells are metabolically abnormal and accumulate FAs and ROS.

Increased FA metabolism and palmitate oxidation distinguish residual cells. To validate the predicted deregulation of key pathways in lipid metabolism (Figure 3A) in vivo, we utilized mammary glands taken from mice 8–10 weeks after achieving a nonpalpable regression state (regressed) along with age-matched control animals. We confirmed the increased expression of several genes involved in the regulation of FA synthesis and oxidative phosphorylation, including cleaved sterol regulatory element-binding protein 1 (SREBP1) and several components of the mitochondrial respiratory chain in the mammary glands of regressed mice (Figure 3B; see complete unedited blots in the supplemental material). The difficulty of studying lipid metabolic enzymes in a fat-embedded epithelium led us to validate Western data with staining of tissue sections. Increased levels of fatty acid synthase (FASN), the key metabolic enzyme for de novo FA synthesis, was confirmed by immunohistochemical staining of mammary glands isolated from regressed and control mice (Figure 3C).

In addition to FASN overexpression, we observed transcriptional increases in the key transcriptional regulator of FA synthesis PPARγ and in the enzymes lipase E (*Lipe*) (Figure 2) and stearoyl-coenzyme A desaturases *Scd1–4*, as well as the FA elongase *Elovl5* and acyl-CoA thioesterase *Acot5* (Supplemental Figure 2, A and B). This stimulated us to investigate differences in FA abundance between never-induced, 5-day-on, and regressed populations. To circumvent the difficulties associated with extracting meaningful data from an epithelium embedded within a fat pad, we performed gas chromatography-mass spectrometry (GC-MS) on lysates from organoid cultures across the 3 time points of interest. Our analysis revealed stark increases in both oleic (C18:1) and myristic (C14) acids (Supplemental Figure 2C). Myristic acid is a saturated FA produced by FASN, supporting our observation of elevated FASN levels in regressed structures and mammary epithelium. Oleic acid is a monounsaturated FA, which is produced through the introduction of a cis double bond at the Δ-9 position of stearic (C18) acid (14). This oxidative conversion of stearic acid to oleic is catalyzed by the NADH-dependent stearoyl-CoA desaturase 1 (SCD1) enzyme, which is also found to be overrepresented in the transcriptomic data. Interestingly, stearic acid appears to accumulate in never-induced cultures, reflecting the lower levels of SCD1 under these conditions. Likewise, the saturated FA palmitate (C16) was found in higher amounts in the never-induced cells, as compared with the regressed state, consistent with the observed increase in the β-oxidation rate in regressed cells (see below).

An increased level of FAs can lead to an increase in lipid droplets, the storage organelle for excess lipids (15). To investigate whether regressed cells had increased stores of triacylglycerides, we utilized the lipophilic dye Nile red, which is nonfluorescent in polar solvents but becomes highly fluorescent in nonpolar environments. Nile red staining is specific for lipid droplets using an excitation of 488 nm/emission 528 nm, while excitation 515 nm/emission > 590 reflects all nonpolar cellular environments. Following staining of regressed structures with Nile red, we observed an appreciable increase in the number of lipid droplets within the regressed organoids (Figure 3D). This observation was confirmed in mammary glands of regressed animals through staining for adipophilin, a lipid droplet–specific marker (Figure 3E).

The observed increase in FA stores suggested that regressed mammary glands were preferentially deriving cellular energy from β-oxidation of FAs. Thus, we determined the flux of 1-^{14}C–labeled palmitate through mitochondrial β-oxidation (16) in mitochondria isolated from mammary glands (Figure 3F). We observed a significant increase in β-oxidative flux of labeled palmitate in mitochondria isolated from the regressed animals for both MYC/KRAS and MYC/NEU models over age-matched controls (Figure 3G). Increased catabolism of FAs via β-oxidative pathways together with the increases in the levels of FASN and other auxiliary pathways of de novo FA synthesis is indicative of a maintenance of a neoplastic lipogenesis phenotype within the population of cells that survive oncogene withdrawal (17).

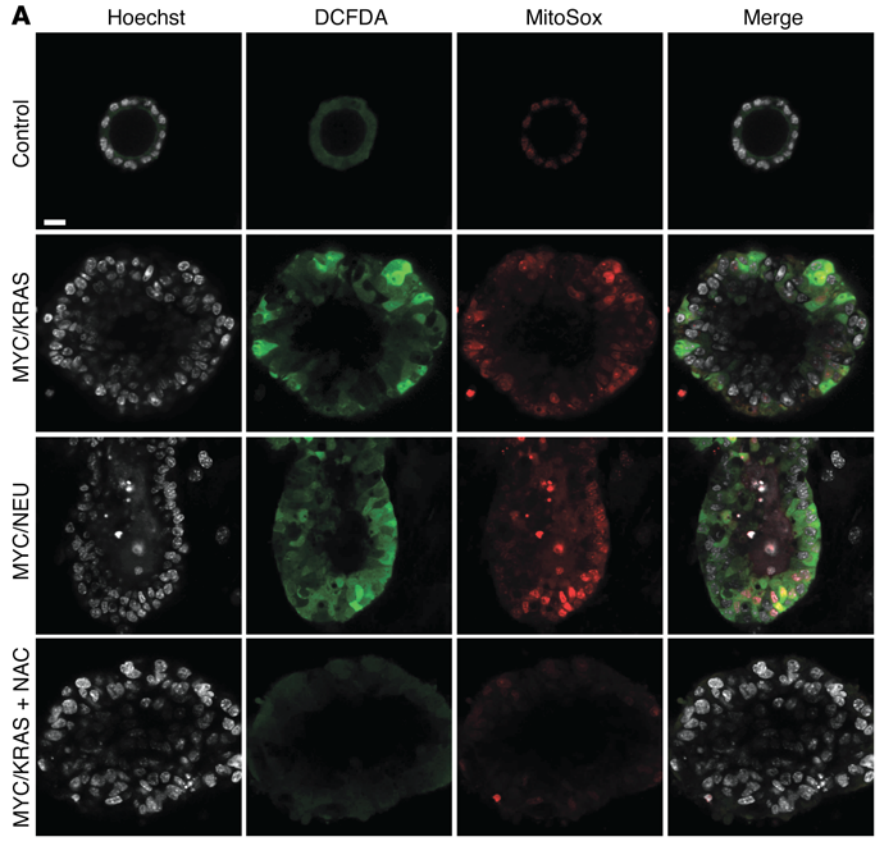

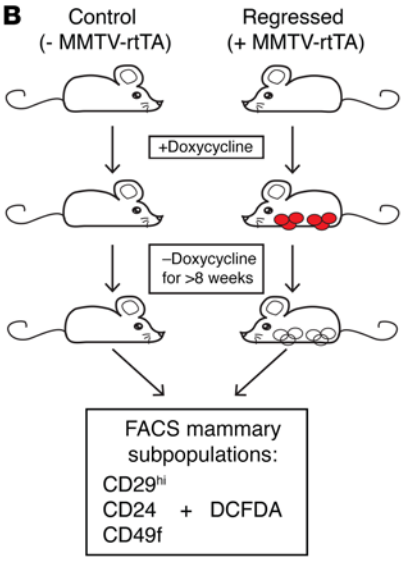

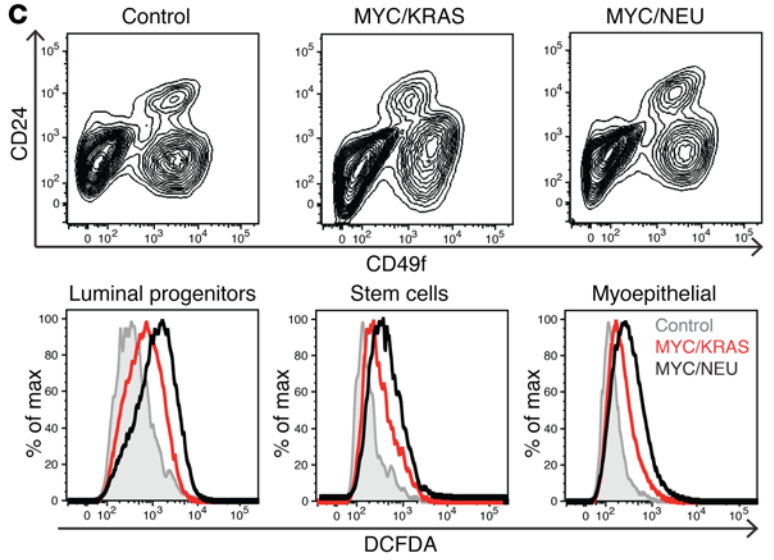

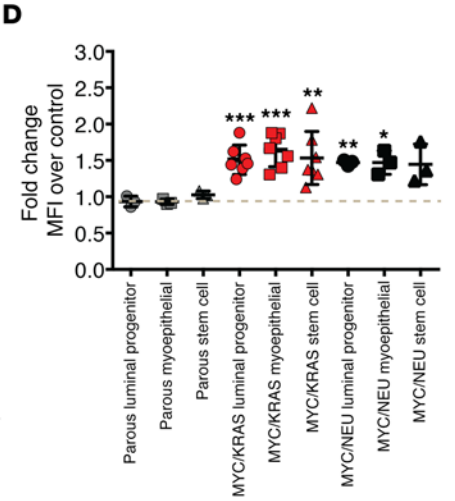

Figure 4. Elevated levels of oxidative stress following oncogene inactivation. (**A**) Staining of organoid cultures with oxidative stress indicator DCFDA (green), superoxide specific MitoSox (red), and DAPI (gray). Single channel and merged representative images of never-induced (control), MYC/KRAS and MYC/NEU structures, and MYC/KRAS structures treated with N-acetylcysteine (NAC). Images are representative of triplicate experiments. Scale bar: 14 μm. (**B**) FACS was performed on regressed and control mice. To control for possible doxycycline effects, mice lacking the reverse tetracycline transactivator were used and placed in experimental cages along with the experimental mice and placed on a diet of chow containing doxycycline. When experimental mice developed a total tumor load of 2 cm^3, all animals, experimental and control, were placed back on normal chow. Animals were maintained on doxycycline-free chow for > 8 weeks before being sacrificed for analysis. Red circles, mammary tumors; white circles, regressed tissue. (**C**) DCFDA was added to previously published FACS-based protocols for separation of mammary epithelial subpopulations. Upper panel: Representative FACS separation of subpopulations using previously published combination of CD29/CD24/CD49f for control, and MYC/KRAS and MYC/NEU regressed mice. Lower panel: Representative histograms the mean fluorescent intensities (MFI) of DCFDA in mammary epithelial cells isolated from age-matched control and regressed animals for the $CD29^{hi}/CD24^{hi}/CD49f^{med}$ (luminal progenitors), $CD29^{hi}/CD24^{med}/CD49f^{med}$ (myoepithelial), and $CD29^{hi}/CD24^{med}/CD49f^{hi}$ (Stem) populations. These results were representative for $n = 9$ (control), $n = 3$ (MYC/NEU), and $n = 6$ (MYC/KRAS) independent experiments. (**D**) Quantification of fold-change of MFI for DCFDA over age-matched control. Parous animals were included as a control for inflammation-driven oxidative stress. Luminal progenitors: MYC/KRAS vs. control, $P = 0.0006$; MYC/NEU vs. control, $P = 0.002$. Myoepithelial: MYC/KRAS vs. control, $P = 0.0003$; MYC/NEU vs. control, $P = 0.03$. Stem: MYC/KRAS vs. control, $P = 0.0084$ enriched populations. One sample t test. Data represented as mean ± SEM; $^*P < 0.05$, $^{**}P < 0.01$, $^{***}P < 0.001$.

Residual cells and mammary glands following oncogene withdrawal contain elevated levels of ROS. The increased flux of FA oxidation in regressed mammary glands, in combination with steady levels of NOXA enzymes and overall transcriptional downregulation of antioxidant enzymes in these cells (Supplemental Figure 3, A and B), further strengthened the prediction that the regressed state exhibits oxidative stress, which we assessed by employing the indicators 2',7'-dichlorofluorescin diacetate (DCFDA), dihydroethidium (DHE), and MitoSOX. Indeed, we observed higher levels of oxidative stress both in the 5-day-on and regressed organoids derived from both models in comparison with the never-induced controls (Figure 4A and Supplemental Figure 3, C and D). Importantly, scavenging by the addition of 20 μM N-acetylcysteine (NAC) confirmed that the indicators indeed sensed ROS (Figure 4A).

To verify the organoid findings in vivo, we isolated cells directly from both regressed and age-matched control mammary glands and analyzed the level of oxidative stress by FACS. In order to address whether elevated ROS was restricted to a specific subpopulation of the mammary epithelium, we utilized an established FACS protocol for separation of mammary epithelial subpopulations (18, 19) together with DCFDA as the ROS indicator (Figure 4B). Interestingly, significantly elevated levels of ROS were detected in the stem cell, myoepithelial, and progenitor populations isolated from regressed mammary glands, suggesting that the elevated ROS is not limited to any one mammary epithelial compartment (Figure 4, C and D).

MYC has recently been shown to play an important role in the regulation of tumor-associated FA oxidative pathways (20). To assess for a MYC-specific memory effect in the regressed population, we evaluated the levels of oxidative stress in mice whose tumors were driven by NEU alone (*TetO-Neu MMTV-rtTA*) and confirmed an increased level of oxidative stress in the regressed mammary glands, despite the absence of MYC, suggesting that the increase in ROS we observed is a general effect associated with oncogene inactivation and not necessarily related to the oncogenotype of the primary tumor (Supplemental Figure 3E).

To exclude that the elevated ROS levels were due to inflammation associated with mammary remodeling following oncogene withdrawal, we used parous mice as a control. Utilizing parous mice that had undergone 3 rounds of pregnancy and weanings, we observed no significant elevation of oxidative stress in any of the parous-derived mammary subpopulations (Figure 4C). In addition, analysis of previously published parity-induced transcriptional changes in mammary cells (GSE40877) showed distinct transcriptional profiles in comparison with our dataset (Supplemental Figure 4, A and B; ref. 21), excluding the possibility that mere tissue architecture remodeling would explain changes in lipid metabolism, cell cycle activity, and oxidative stress in the regressed cell population.

In summary, we found clear signs of oxidative stress in the regressed state of both organoids and mammary glands of breast cancer mouse models following oncogene withdrawal.

Lapatanib treatment results in elevated ROS and lipid storage. The preclinical mouse models used in this study theoretically mimic a perfect therapeutic setting, since the expression of the driving oncogenes is both spatially and temporally regulated by the addition or exclusion of doxycycline. Organoid cultures derived from this system have allowed us to model and characterize an MRD correlate state, which displays heightened oxidative stress and increased lipid stores in comparison with never-induced cells. This finding has been confirmed in mammary glands derived from regressed mice. However, these results do not completely reflect the clinical setting where the disease is managed through administration of systemic adjuvant therapies. To address this in the organoid culture, we treated organoids overexpressing MYC/NEU with the NEU tyrosine kinase inhibitor lapatinib.

Similar to the oncogene inactivation setting, treatment with lapatinib resulted in a rapid clearing of the organoids, despite the continuous administration of doxycycline, with persistence of a regressed population. We stained the population of cells surviving the pharmacological treatment for FASN, ROS, and lipid droplet accumulation (Supplemental Figure 5) to correlate them with the oncogene-inactivated structures (Figure 3, C and D, and Figure 4A) and observed an increase in FASN protein levels as seen in immunofluorescence. Additionally, increased lipid stores and ROS were observed in regressed lapatanib-treated structures similar to the oncogene-inactivated counterparts. The lack of lipid droplet accumulation or elevated ROS in the lapatinib-treated never-induced control cells excluded the possibility of off-targets being responsible for the effects seen in the lapatinib-regressed organoids. We conclude that inactivation of the oncogenes, utilizing the described inducible system, results in a regression comparable with that obtained with pharmacologic inhibition.

Aberrant lipid metabolism drives oxidative DNA damage following oncogene inactivation. Increased levels of oxidative stress can cause damage to nucleic acids, proteins, and lipids and can also affect cellular signaling (22). Oxidative stress has long been implicated in aging and tumorigenesis, making it a good candidate for driving the dormant population of residual cells toward tumor recurrence. To test if the higher levels of ROS led to oxidative DNA damage, we performed immunofluorescence on mammary glands of regressed and control mice for the presence of FASN together with 8-Oxo-2'-deoxyguanosine (8-OHdG), one of the major products of DNA oxidation. Despite no appreciable increase in global levels of γH2AX, we observed elevated levels of 8-OHdG in regressed mammary glands from both MYC/KRAS and MYC/NEU models compared with controls (Figure 5A and Supplemental Figure 6, A and B). Given the adduct specificity of 8-OHdG, we confirmed the general presence of oxidized DNA utilizing a modified comet assay including formamidopyrimidine DNA-glycosylase. Indeed, we again observed an increase in the percentage of DNA damage in the regressed population (Supplemental Figure 6C), despite an increased initiation of base excision repair (BER; Supplemental Figure 6D).

We have demonstrated that an MRD correlate state is characterized by elevated oxidative stress and DNA adducts. The potential to disrupt proposed drivers, FASN and fatty acid β-oxidation, of these hallmarks provides an attractive therapeutic avenue in the prevention of tumor recurrence. To test this hypothesis in vitro, following oncogene inactivation, 2 small molecules — C75 and etomoxir — were administered to organoid cultures to explore their effects on ROS and adduct formation.

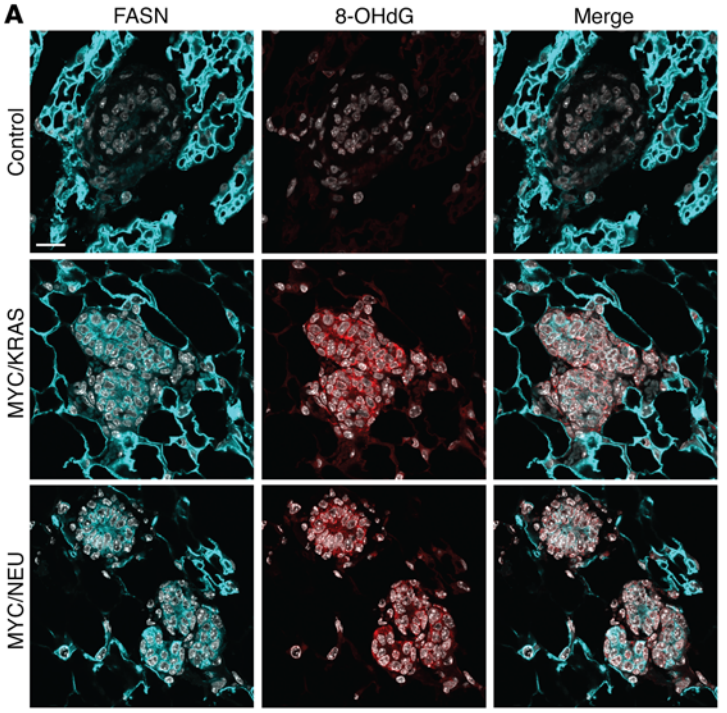
A
FASN
8-OHdG
Merge
Control
MYC/KRAS
MYC/NEU

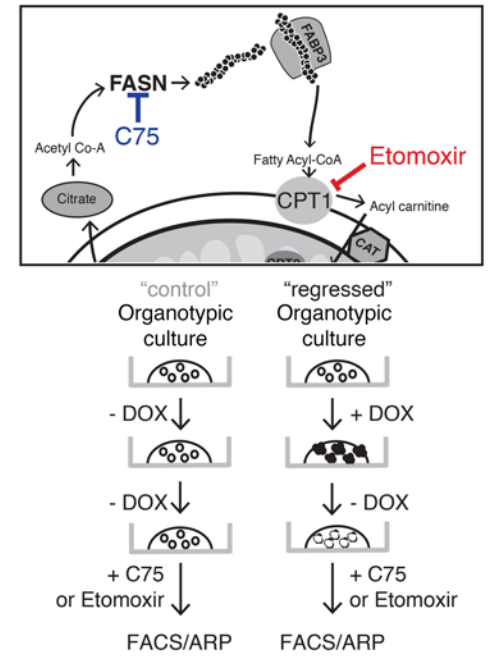
B
FABP3
FASN
C75
Acetyl Co-A
Fatty Acyl-CoA
Etomoxir
Citrate
CPT1
Acyl carnitine
CAT
"control" Organotypic culture
"regressed" Organotypic culture
- DOX
+ DOX
- DOX
- DOX
+ C75 or Etomoxir
+ C75 or Etomoxir
FACS/ARP
FACS/ARP

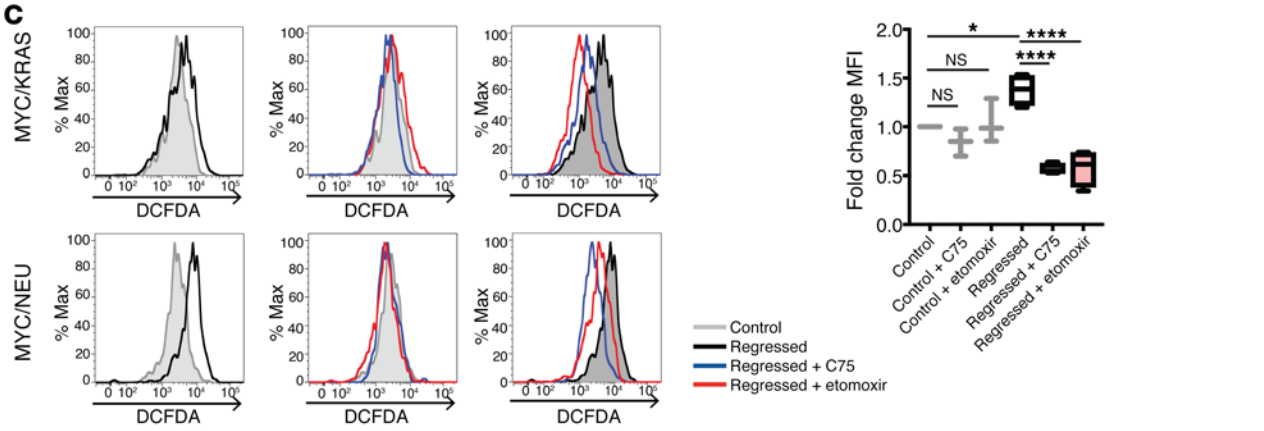
C
MYC/KRAS
MYC/NEU
% Max
DCFDA
Control
Regressed
Regressed + C75
Regressed + etomoxir
Fold change MFI
NS
NS
*
****
****
Control
Control + C75
Control + etomoxir
Regressed
Regressed + C75
Regressed + etomoxir

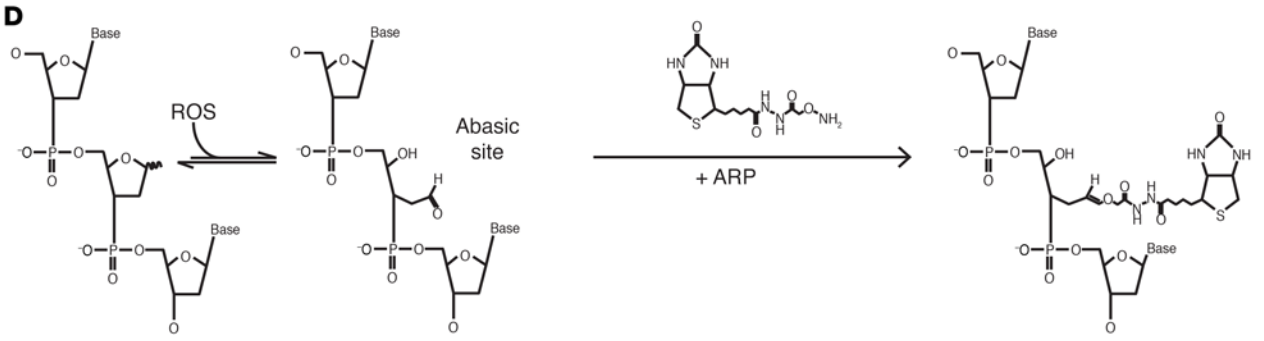
D
Base
ROS
Abasic site
+ ARP

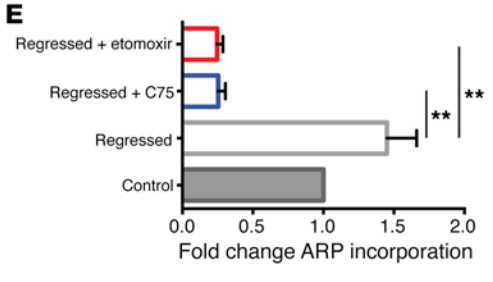
E
Regressed + etomoxir
Regressed + C75
Regressed
Control
**
**
Fold change ARP incorporation

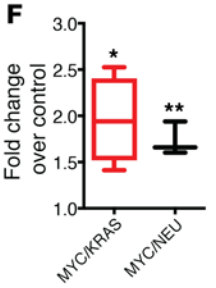
F
Fold change over control
*
**
MYC/KRAS
MYC/NEU

Figure 5. Inhibitors of lipid metabolism abrogate oxidative DNA damage in regressed cells. (**A**) Confocal microscopy imaging of control and regressed mammary tissue stained for FASN (cyan), 8-hydrox-deGuaninine (8-OHdG; red), and DAPI (gray). Scale bar: 15 μm. (**B**) To causally link lipid metabolism to oxidative stress, organoid cultures were treated with C75 or etomoxir after oncogene withdrawal with 100 μm etomoxir or 0.6 μg/ml C75 for 24 hours. Following a 24-hour incubation, cells were assessed by DCFDA (FACS) and/or subjected to aldehyde reactive probe (ARP) assay (see below). (**C**) FACS of cells derived from treated organoid cultures. Upper panels: Representative histograms showing the difference in DCFDA control (gray) and regressed (black) organoids derived from MYC/KRAS and MYC/NEU mice. Middle panels: Representative histograms of control samples (gray) treated with C75 (blue) and etomoxir (red). Lower panels: Representative histograms of regressed samples (black) treated with C75 (blue) and etomoxir (red). Mean fold-change for (n = 3) control and (n = 4) regressed independent experiments is represented on the right. Regressed (P = 0.0189); regressed + C75 (P < 0.0001); regressed + etomoxir (P < 0.0001). One-way ANOVA with Sidak multiple comparison test. (**D**) ARP assay for base-excision repair intermediates. Detection of the apurinic/apyrimidinic sites is achieved through use of a biotinylated probe that binds the exposed aldehyde present in the AP site. Quantification is done using streptavidin-HRP. (**E**) Quantification of ARP assay represented as fold-change of ARP incorporated into the DNA isolated from C75- and etomoxir-treated and untreated regressed organoids (n = 2) and control (n = 2) untreated organoid cultures. Regressed + C75 (P = 0.0019); regressed + etomoxir (P = 0.0014). One-way ANOVA with Dunnetts multiple comparison test. (**F**) Quantification ARP assay represented as fold-change of ARP incorporated into the DNA isolated from experimental animals over age-matched controls. Represented for MYC/KRAS (P = 0.025), n = 4; MYC/NEU (P = 0.036), n = 3; control, n = 4 animals; one sample t test. Data represented as mean ± SEM; *P < 0.05, **P < 0.01, ****P < 0.0001.

C75 (4-methylene-2-octyl-5-oxotetra-hydrofuran-3-carboxylic acid) is a semisynthetic inhibitor of FASN that functions through binding of the β–ketoacyl synthase subunit. FAs are synthesized by FASN through addition of Acetyl-CoA to Malonyl-CoA via an NADPH-dependent condensation step. This reaction is carried out by the β–ketoacyl synthase subunit of FASN; the binding of C75 results in the obstruction of FA synthesis. Downstream, etomoxir inhibits mitochondrial FA β-oxidation by irreversibly binding carnitine palmitoyltransferase 1 (CPT1) and preventing entry of long-chain FAs into the mitochondria (Figure 5B).

Following 24 hours of treatment, we observed a significant reduction in oxidative stress, as measured by DCFDA in FACS analysis, in the populations of regressed cells treated with either inhibitor; the control groups remained largely unchanged (Figure 5C).

Next, we verified whether the observed reduction of overall oxidative stress could be translated to a reduction in adduct formation in the treated cultures. In order to retain genomic integrity, DNA adducts are usually resolved by the BER pathway. In BER, the excision of an adduct results in the formation of an apurinic/apyrimidinic (AP) site, which can be detected using a biotinylated aldehyde reactive probe (ARP) that reacts with the aldehyde ring of the opened AP sites (Figure 5D; refs. 23, 24). This assay clearly showed a significant increase in ARP incorporation in the regressed samples compared with control (Figure 5, E and F). However, following treatment with either C75 or etomoxir, significant reductions in ARP incorporation were observed for DNA isolated from treated regressed cultures (Figure 5E). Taken together, the efficacy of both C75 and etomoxir to decrease overall ROS and AP site incidence in regressed mammary glands is consistent with our proposal that increased FA metabolism drives the acquisition of ROS-driven point mutations. Intriguingly, these results suggest that the inclusion of drugs targeting FA catabolism in adjuvant settings could improve long-term survival rates for breast cancer survivors.

Reducing ROS levels and proliferation of mammary epithelium attenuates recurrence in vitro and in vivo. During the ovarian estrous cycle, the mammary gland undergoes remodeling accompanied by expansion of the stem and luminal progenitor compartments (Figure 6A; ref. 25). We have demonstrated above that regressed mammary glands harbor higher levels of oxidative DNA damage. Oxidative DNA damage is highly mutagenic, with incorrect base insertion during replication being the most common mechanism of ROS-driven mutagenesis. Hormone-driven proliferation of the mammary epithelium, which occurs during every estrous cycle, forces residual cells (elevated in adduct-potentiating ROS) to divide and is, thus, likely to be an important driver for promoting acquisition of somatic mutations and recurrence.

As previously mentioned, the regressed structures are largely dormant, with very low Ki67 positivity (Supplemental Figure 1A). Therefore, to test the effect of targeted ROS therapy (by supplementing NAC) on the onset of recurrence, we recapitulated the hormonal cycle–induced expansion in vitro by serial reseeding of the regressed organoids. To that end, the regressed and never-induced organoids were singularized and reseeded into fresh Matrigel. With each reseeding, a subset of cells divided and formed new organoid structures. These reseeded organoids were cultured in either normal media or in the presence of NAC. Analysis of reseeded organoids indicated that, in comparison with the reseeded never-induced cultures, the regressed reseeded cells displayed a NAC-independent persistence of increased FASN expression and lipid droplet accumulation (Supplemental Figure 7A), suggesting that altered lipid metabolism is a stable phenotype in this population.

Following an average of 4 reseedings, we detected spontaneous relapses only in organoids derived from reseeded regressed structures that could be propagated as solid-growing in vitro relapses (Figure 6B). Sequencing of independent in vitro relapses revealed newly acquired mutations within the rtTA region that render them independent of doxycycline and lead to reexpression of the original oncogenes (Supplemental Figure 7B; ref. 5). Moreover, injection of cells from in vitro relapses into the cleared mammary fat pad of *Rag1*$^{-/-}$ mice resulted in the formation of tumors closely resembling in vivo relapses from the same mice (Supplemental Figure 7C). To test if ROS have a causal role in generating de novo somatic mutations and relapse, we reseeded cells as described above in the presence of the ROS scavenger NAC. This resulted in a near-complete abrogation of in vitro relapses (Figure 6B).

The findings from our ex vivo organoid culture highlighted the importance of proliferation for driving somatic mutation acquisition and tumor recurrence from a residual cell population. These observations prompted us to develop a 2-pronged strategy for attenuating tumor recurrences in vivo, either by scavenging ROS or through elimination of the hormone-driven proliferation of the mammary gland (26, 27). Following a round of oncogene-induced tumorigenesis and full regression to nonpalpable state by oncogene withdrawal, mice were either treated with the ROS scavenger

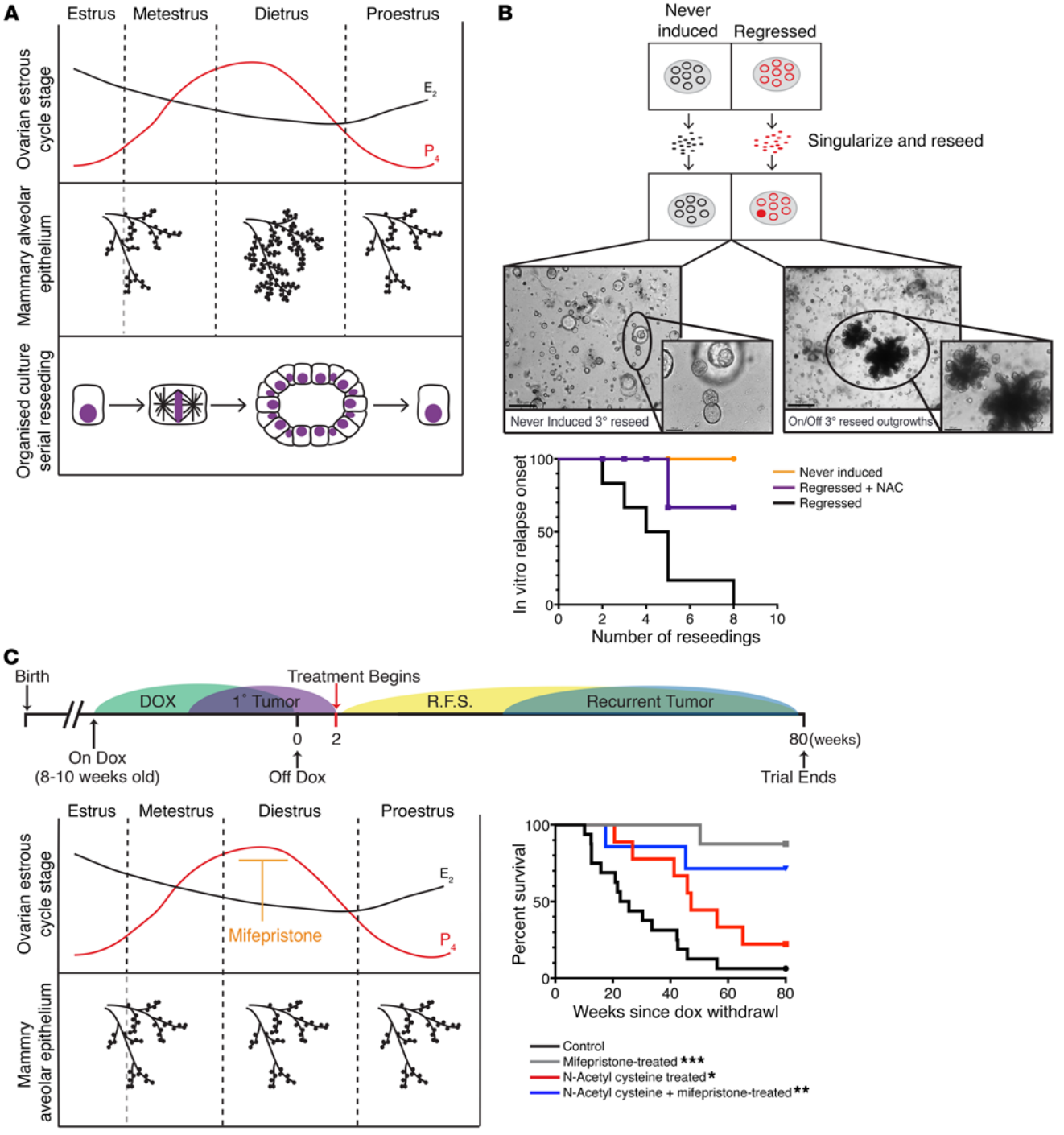

Figure 6. Progesterone antagonists and ROS scavengers attenuate tumor recurrence. (**A**) The nonpregnant adult mammary gland undergoes profound morphological changes during the ovarian estrous cycle. A specific 2-fold expansion of the alveolar branching coincides with the peak in progesterone during diestrus. The hormone-driven induction of proliferation can be recapitulated in vitro through serial reseeding of organoid cultures. Reseeding of singularized cells stimulates de novo proliferation, resulting in the formation of acinar structures, similar to initial acini formation. (**B**) Generation of in vitro relapses through continuous reseeding of singularized cells. Represented as relapse-free persistence for never-induced, regressed, and regressed + N-acetylcysteine (NAC) (20 μM) populations; $n = 6$ independent experiments. Lower panel: Representative brightfield images of acinar structures from serially reseeded cultures at the third reseeding for hollow never-induced structures and corresponding regressed structures with first appearance of in vitro relapse. Scale bar: 50 μm. (**C**) Attenuation of tumor recurrence following treatment with progesterone antagonists and ROS scavengers. Upper panel: Experimental timeline in which MYC/KRAS regressed mice were treated with NAC, mifepristone, or the combination of NAC/mifepristone. Treatment began 2 weeks following oncogene inactivation and continued until spontaneous recurrence or 80 weeks after oncogene inactivation. Lower left panel: Role of mifepristone, a progesterone-receptor modulator that blocks hormone-driven expansion of the mammary gland. We postulated that cessation of proliferation would result in a decrease in somatic mutations generated via replication through oxidative DNA adducts, subsequently lowering the rate of tumor recurrence. The survival curve (lower right) represents relapse-free survival percentages for the 4 cohorts of mice treated with NAC, mifepristone, or the combination of NAC/mifepristone, as well as control nontreated. Significance was calculated using the log-rank (Mantel-Cox) test confronting NAC cohort, $P = 0.0342$; mifepristone cohort, $P = 0.0004$; and NAC + mifepristone cohort, $P = 0.0039$ with untreated. No significant difference was seen noted between the 2 mifepristone containing cohorts $P = 0.3995$. $^{*}P < 0.05$, $^{**}P < 0.01$, $^{***}P < 0.001$.

NAC, the progesterone antagonist mifepristone, or a combination of mifepristone and NAC. We have employed the use of mifepristone as a progesterone antagonist in our studies to halt the expansion of the mammary alveolar epithelium that coincides with the peak in progesterone during diestrus of the ovarian estrous cycle (Figure 6, A and C; ref. 28). Mifepristone has been successfully used in a similar setting in the prevention of BRCA1-mediated tumorigenesis (27) and is currently under evaluation in a phase 2 clinical trial (NCT01898312) for its effectiveness in eliminating ovarian estrous cycle–driven breast cell proliferation in a preventive setting for patients harboring germline BRCA1/2 mutations. Despite diminished/reduced scavenging toward the end of the weekly treatment schedule (Supplemental Figure 7D), NAC-only–treated animals had a significant delay in the onset of tumor recurrence (Figure 6C), while relapse onset was nearly abrogated in both the mifepristone and the combined mifepristone and NAC treatment cohorts (Figure 6C and Supplemental Figure 7E). These findings demonstrate, both in vivo and in vitro, that ROS scavenging has a beneficial effect on prevention of tumor relapse and, coupled with prevention of hormone-driven proliferation, may provide a new opportunity for therapeutic intervention to attenuate spontaneous tumor recurrences.

Elevated FA metabolism is a communal hallmark of cells surviving neoadjuvant treatment in human breast cancer patients. Neoadjuvant therapeutic approaches may be delivered to breast cancer patients to induce downstaging, thus rendering a locally advanced tumor operable, but they also provide the advantage of allowing the study of the effect of systemic therapies on tumor survival (29). Transcriptome analysis of tumors before and after successful neoadjuvant therapy should provide the gene expression signature of residual cells (30). To that end, we performed RNA-seq on 7 matched cases of preneoadjuvant treatment core biopsies and posttreatment surgical samples (ArrayExpress database; E-MTAB-4632)(Supplemental Table 3). Furthermore, we reanalyzed the previously published human dataset (GSE32072) and compared both human datasets to our mouse-derived regressed mammary duct organoid datasets for the 5-day-on versus regressed comparison, resembling the neoadjuvant setting.

Focusing on the gene sets that were overrepresented in the treated versus pretreated samples, we employed reactome pathway enrichment analysis to evaluate the degree of overlap of the transcriptional response between the mice and the 2 human datasets (Supplemental Figure 8 and Supplemental Table 4). Considering that datasets were not stratified for intrinsic tumor subtype, treatment, or grade together with the general difficulties in performing interspecies comparisons, we expected a minimal overlap between significantly regulated pathways in this comparison. However, the analysis revealed pathways that were highly reminiscent of the defining features of MRD described in this manuscript for the mouse models. Specifically, we found a number of overlapping pathways between human datasets and our model systems that pertained to lipid metabolism and redox maintenance (Supplemental Figure 8 and Supplemental Table 4). The presence of lipid metabolic pathways in this analysis supported the finding of dysregulated lipid metabolism as a central hallmark of cells that survive therapeutic intervention. To gain further insight, we plotted the metabolism of lipids and lipoproteins reactome landscape for the significant up- and downregulated pathways over the human and mouse datasets (Figure 7). The high degree of commonality in lipid metabolic pathways found to be conserved between our mouse model–derived dataset and the MRD patient samples provided further support for dysregulated lipid metabolism as a hallmark of cells that survive therapeutic intervention.

The predominance of lipid metabolic pathways within the pathway analyses drove us to search for common predicted metabolites between the mouse and human datasets. To do so, we applied the previously described reporter metabolite analysis (Figure 2) to both human datasets and the organoid-derived datasets. Again, we noted a high degree of overlap in predicted metabolites across all datasets (Supplemental Figure 8 and Supplemental Table 5). In accordance with both of our previous observations, a large number of the top-scoring reporter metabolites identified in human as well as mouse datasets were associated with lipid metabolism. Specifically, several fatty-acyl CoAs were predicted to be enhanced in all cases. Further, PPARα, a transcription factor activated by FA derivatives that also regulates the expression of a large number of genes involved in FA β-oxidation, was also predicted to be active.

In order to determine whether the predictions based on transcriptional signatures translated to the protein level, we obtained patient samples from NEU$^+$, luminal A/B-like, and triple-negative subtypes of breast cancer prior to and following pertinent neoadjuvant treatments. We verified elevated expression of both FASN and 8-OHdG in the samples following treatment (Figure 8, A and B, and Supplemental Figure 9, A and B), despite having a proliferative index comparable with that of the healthy breast controls (Supplemental Figure 9C). Interestingly, the elevated levels of FASN were observed independently of tumor type and/or treatment regimen (Supplemental Table 6). Collectively, given the progressive nature of the disease (Supplemental Figure 9D), these data indicate that perturbation of lipid metabolism has clinical relevance in addressing cancer progression from MRD in breast cancer patients.

Discussion

Despite their transcriptional and mutational heterogeneity, cancer cells derived from different tumor types often have similar metabolic abnormalities, including the shifts of energy metabolism from oxidative phosphorylation to aerobic glycolysis, increases in protein and nucleotide synthesis, and augmented FA synthesis, FA storage, and metabolism (17, 31–34). However, little attention has been paid to the metabolic signature of MRD after therapy.

In this study, we used a combination of 2 mouse models of oncogene-driven breast cancer, together with the respective organoid cultures, to obtain pure transcriptional signatures of the population of cells that survive oncogene inactivation. The transcriptome signature of these cells indicated a failure to reestablish a transcriptional baseline state, reflecting either a tumorigenic memory or a potential survival signature. In-depth characterization of the signatures revealed a decrease in proliferative capacity, along with an altered energy metabolism.

In line with our data, transcriptome analysis of samples from recipients of neoadjuvant therapy revealed that, when cancers were

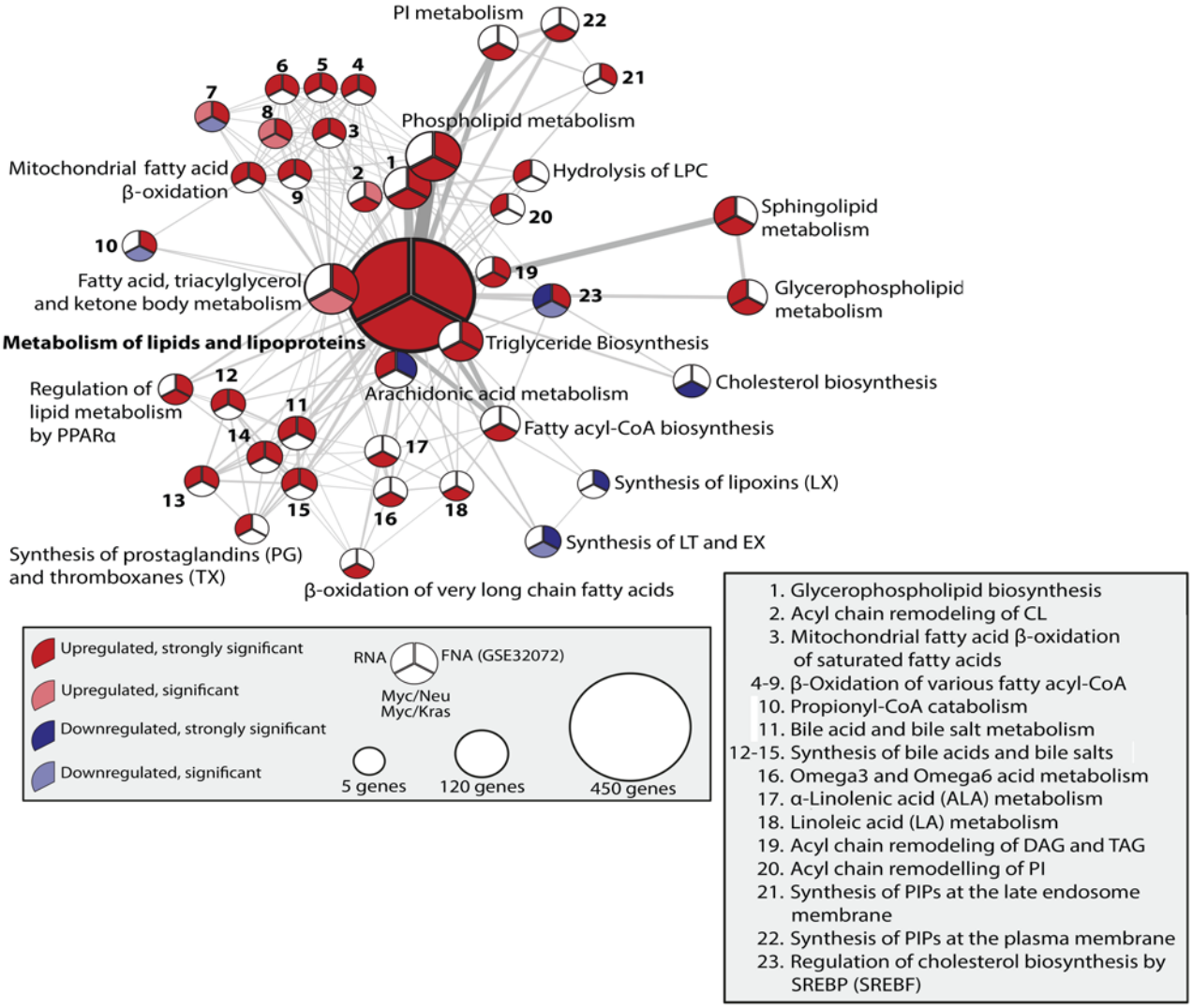

Figure 7. Lipid phenotype of neoadjuvant-treated breast cancers. Network plot for all reactome pathways under the term "Metabolism of lipids and lipoproteins," which are significantly deregulated in at least one of 4 assays: MYC/KRAS, MYC/NEU, GSE32072, or RNA-seq. Strong significance threshold for mouse assays, $P < 0.005$, and human assays, 0.05. Significance threshold for mouse assays, $P < 0.05$, and human assays, $P < 0.1$. Pathway significance is colored by its best P value in the mouse assays.

analyzed without stratification, PPAR signaling was the most statistically significant deregulated pathway in the residual cancer cells (30). Notably, aberrant FA ametabolism was detected in MRD across all the breast cancer intrinsic subtypes, an observation supported by positive FASN staining of neoadjuvant-treated patient samples.

Alterations in lipid metabolism have previously been shown to be a hallmark of breast cancer, with increased overexpression of some key genes correlating with disease progression (35, 36). Recently, alterations in energy metabolism have also been shown to be a hallmark of cells that have survived $KRAS^{G12D}$ inactivation in pancreatic cancer (37). However, the mechanism by which altered metabolism could drive relapse had not been addressed. In this study, we demonstrate that regressed mammary glands have higher levels of FA metabolism. Through direct perturbation of FA metabolism using C75 and etomoxir, we established that dysregulated lipid metabolism drives elevated oxidative stress and increased DNA adduct formation in MRD. Attenuation of somatic mutation–driven tumor recurrence via the use of antioxidants further supports the causal role of an unchecked lipid metabolism in driving tumor recurrence.

Our results support that these characteristics would accelerate somatic mutation–driven tumor recurrences and that this effect is strongly potentiated in a hormone-responsive organ. Our demonstration that mifepristone successfully delayed tumor recurrence highlights the possibility of a correlation between hormone-driven proliferation and tumor recurrence. Indeed, one of the major independent risk factors for local tumor recurrence in women who have received breast-conserving therapy is "young" age (premenopausal [<50]; refs. 38, 39). Studies have also highlighted a strong association between progesterone-containing hormone replacement therapy (HRT) treatment and tumor recurrence. The 3 randomized trials, Hormonal Replacement After Breast Cancer - Is It Safe (HABITS), Livial Intervention following Breast Cancer: Efficacy, Recurrence, And Tolerability Endpoints

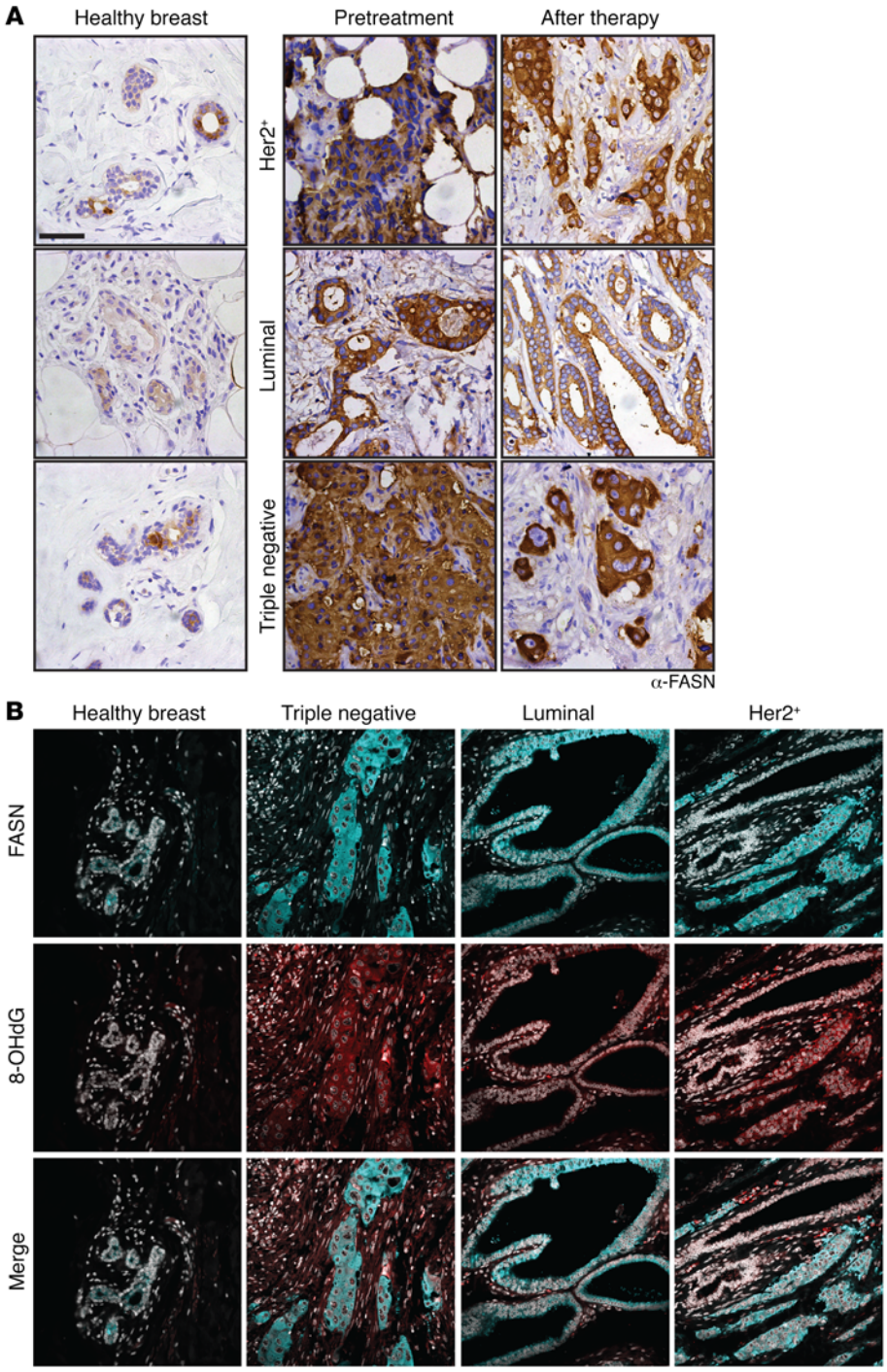

Figure 8. Postneoadjuvant–treatment human breast cancer samples display elevated FASN and 8-OHdG levels. (**A**) IHC of healthy mammary tissue and matched preneoadjuvant- and postneoadjuvant-treatment human breast cancer samples for FASN. The images, showing enhanced staining in the tumor samples, are representative for (n = 11) luminal, (n = 10) HER2 3+, and (n = 9) triple negative patient samples for each subtype. HER2 3+, treatment regimen Herceptin + combined hormone therapy (CHT); luminal, aromatase inhibitor; triple negative, CHT. Samples from patients, which were classified as responsive to the neoadjuvant therapy, were chosen for analysis. Scale bar: 50 μm. (**B**) Immunofluorescence staining of of preneoadjuvant- and postneoadjuvant-treatment human breast cancer samples; FASN (cyan), 8OHdG (red), DAPI (gray). The images are representative of (n = 10) patient samples for each subtype. HER2 3+, treatment regimen herceptin + CHT; luminal, aromatase inhibitor; triple negative, CHT. Samples from patients, which were classified as responsive to the neoadjuvant therapy, were chosen for analysis.

(LIBERATE), and Stockholm trials, of HRT treatment in women with a previous history of breast cancer had to be halted due to concerns about the safety of the treatment following early follow-ups (40–42). Although — even in healthy individuals — late onset of menopause, early menses, and HRT are all associated with a risk in developing breast cancer (43, 44), cyclical expansion of the mammary gland (25) could hasten the acquisition of secondary mutations that drive relapse in breast cancer survivors harboring a mutation-permissive metabolism.

Although not as dramatic as the effect seen with mifepristone, we did see a significant attenuation of tumor recurrence in mice treated with ROS scavenger NAC. This raises the question of whether it would be beneficial to evaluate the inclusion of antioxidants in a preventive setting following surgical and therapeutic intervention. Supplementation of cytotoxic antitumor therapy regimes with antioxidants has been the subject of many studies (45, 46). There are numerous and conflicting reports concerning the effects of inclusion of antioxidants on overall survival or clinical response; however, these studies are largely addressing the potential of antioxidants, such as vitamins, to interfere with cytotoxic therapies that traditionally rely upon oxidative stress mechanisms to inflict damage on existing cancer cells.

In this study, antioxidants were administered as an adjuvant therapy after initial therapeutic intervention. Very few studies have focused on evaluating the influence of vitamin supplementation on long-term outcomes among breast cancer patients. Interestingly, 2 independent prospective cohort studies reported that increased dietary supplementation of vitamins C and E, during the period following cancer diagnosis, confers a protective effect in regard to tumor recurrence and overall survival in breast cancer patients (47, 48). This supports our observations that the use of antioxidants in an adjuvant setting can bestow a survival advantage. The factors governing the efficacy of vitamin supplementation, including effective serum levels and interaction with therapy, is likely to be very complex. However, considering the potential for benefits, it is one that deserves further attention.

Here, we present an approach that combines complementary in vivo and ex vivo systems for characterization of the substrate of breast cancer recurrence. We report a differential energy metabolism, which is active in at least a subpopulation of the surviving cells, and show that these cells have the capability acquiring de novo somatic mutations after oncogene inactivation. It is apparent from our combined computational and cellular approaches that increased lipid metabolism is a metabolic hallmark of cells surviving therapeutic treatment that transcends the etiological differences among human breast tumor subtypes. The commonality of this hallmark strongly suggests that altered energy metabolism could be an Achilles heel for interfering with cancer progression toward relapse and is an attractive subject for future mechanistic and clinical studies.

Methods

Supplemental Methods are available online with this article.

Animals. All the mice were bred and maintained in the EMBL Mouse Biology Unit, Monterotondo, in accordance with Italian legislation and under license from the Italian Health Ministry. Mice were housed under barrier conditions with 12-hour light/12-hour dark cycles. We utilized the following mouse strains: *TetO-cMYC TetO-KrasG12D MMTV-rtTA* as described in ref. 5 and *TetO-Neu MMTV-rtTA* as described in ref. 6.

Tristransgenic *TetO-cMYC TetO-Neu MMTV-rtTA* and *TetO-cMYC TetO-KrasG12D MMTV-rtTA* and bitransgenic *TetO-Neu MMTV-rtTA*, *TetO-cMYC TetO-KrasG12D*, and *TetO-cMYC TetO-Neu* (TT+) control mice were generated, and tumors were induced through the activation of transgene expression, which was achieved by administration of a doxycycline supplemented diet (625 mg/kg doxycycline; Mucedola). Control mice (TT+) were placed on doxycycline, along with experimental animals at 8–10 weeks of age for 30 days; they were then taken off and placed on a normal diet.

Data deposition. Datasets generated as a part of this study were deposited at ArrayExpress with the following accession numbers: E-MTAB-3038, E-MTAB-3039, and E-MTAB-4632. Please refer to Supplemental Methods.

Statistics. Graph Pad Prism, version 7.1 (GraphPad Software) was used for generating graphs and preforming statistical tests. This study has employed the use of Student *t* tests for determining significance between related comparisons; for multiple comparisons, one-way ANOVA was followed by Dunnett's or Sidak multiple comparison tests. Log-rank Mantel Cox tests were utilized for analyzing significance in relapse-free survival. *P* values of less than 0.05 were considered statistically significant. Data presented in figure legends is represented as mean ± SEM unless otherwise stated; statistical tests utilized are reported in the figure legends, along with the associated *P* values.

Study approval. Regarding neoadjuvant-treated patient samples for RNA-seq, the study entitled "Ermittlung neuer Zielproteine für kombinatorische Therapien bei Brustkrebs-Patientinnen sowie die Entwicklung prognostischer und prädiktiver Markerprofile" with the study number S-039-2008 was approved by the Ethical Committee of the Medical Faculty in Heidelberg.

Regarding human breast samples for IHC analysis, the patients were not selected for a clinical trial specifically. All patients came from clinical practice, prospectively entered the European Institute of Oncology breast cancer database, and gave an informed consent for using their clinico-pathological data and samples for research purposes at the time of admission to the hospital. The proceedings were approved by the IEO Review Board.

Author contributions

KMH and MJ designed the experiments. KMH carried out the experiments. JS cultured cells and isolated RNA for affymetrix analysis. VM and BK performed comparison with GSE32072. BK analyzed the RNA-seq data. VM and KRP ran reporter metabolite analysis. KR and EK performed the GC-MS analysis. KR, AA, and MG performed experiments and stainings. TJG and KRP supervised the computational work. BB and AS provided human samples for RNA-seq. GP and NR provided human samples for histology. KMH and MJ wrote the manuscript. MJ and RS supervised the work.

Acknowledgments

We thank Jelena Pistolic for technical assistance in preparation and hybridization of the samples to the affymetrix platforms; Federico Villa for assistance with tissue culture and sample preparation; Cora Chadwick and Daniel Bilbao for expert assistance with FACS sorting; Giuseppe Chiapparelli for mouse husbandry; Prasad Phapale and the Metabolomics Core Facility for expert assistance; Grischa Tödt for suggestions toward probe reannotation of the array datasets; and Donal O'Carroll, Darren Gilmour, and Jan Ellenberg for critical readings of the manuscript. This study was technically supported by EMBL Monterotondo Microscopy Facility and the Laboratory for Animal Resources. KMH was supported by the EMBL Interdisciplinary Postdoc Program under Marie Curie COFUND Actions. Work in RS's laboratory is supported by the European Research Council under the European Union's Seventh Framework Programme (FP7-2007-2012)/ERC grant agreement number ERC-281614, Marie Curie PCIG09-GA-2011-293745, and the Howard Hughes Medical Institute. Work in MJ's laboratory is supported by Marie Curie PCIG-GA-2011-294121, 3DBreastCancer.

Address correspondence to: Martin Jechlinger, EMBL Heidelberg, Cell Biology and Biophysics unit, Meyerhofstraße 1, 69117 Heidelberg, Germany. Phone: 49.6221.3878401; E-mail: martin.jechlinger@embl.de.

JS's present address is: University of Basel Medical Faculty, Basel, Switzerland.

1. Klein CA. Framework models of tumor dormancy from patient-derived observations. *Curr Opin Genet Dev*. 2011;21(1):42–49.
2. Aguirre-Ghiso JA. Models, mechanisms and clinical evidence for cancer dormancy. *Nat Rev Cancer*. 2007;7(11):834–846.
3. Hartkopf AD, et al. The presence and prognostic impact of apoptotic and nonapoptotic disseminated tumor cells in the bone marrow of primary breast cancer patients after neoadjuvant chemotherapy. *Breast Cancer Res*. 2013;15(5):R94.
4. Politi K, Pao W. How genetically engineered mouse tumor models provide insights into human cancers. *J Clin Oncol*. 2011;29(16):2273–2281.
5. Podsypanina K, Politi K, Beverly LJ, Varmus HE. Oncogene cooperation in tumor maintenance and tumor recurrence in mouse mammary tumors induced by Myc and mutant Kras. *Proc Natl Acad Sci U S A*. 2008;105(13):5242–5247.
6. Moody SE, et al. Conditional activation of Neu in the mammary epithelium of transgenic mice results in reversible pulmonary metastasis. *Cancer Cell*. 2002;2(6):451–461.
7. D'Cruz CM, et al. c-MYC induces mammary tumorigenesis by means of a preferred pathway involving spontaneous Kras2 mutations. *Nat Med*. 2001;7(2):235–239.
8. Jechlinger M, Podsypanina K, Varmus H. Regulation of transgenes in three-dimensional cultures of primary mouse mammary cells demonstrates oncogene dependence and identifies cells that survive deinduction. *Genes Dev*. 2009;23(14):1677–1688.
9. Huber W, von Heydebreck A, Sültmann H, Poustka A, Vingron M. Variance stabilization applied to microarray data calibration and to the quantification of differential expression. *Bioinformatics*. 2002;18(Suppl 1):S96–S104.
10. Leek JT, Johnson WE, Parker HS, Jaffe AE, Storey JD. The sva package for removing batch effects and other unwanted variation in high-throughput experiments. *Bioinformatics*. 2012;28(6):882–883.
11. Patil KR, Nielsen J. Uncovering transcriptional regulation of metabolism by using metabolic network topology. *Proc Natl Acad Sci U S A*. 2005;102(8):2685–2689.
12. Zelezniak A, Pers TH, Soares S, Patti ME, Patil KR. Metabolic network topology reveals transcriptional regulatory signatures of type 2 diabetes. *PLoS Comput Biol*. 2010;6(4):e1000729.
13. Thiele I, et al. A community-driven global reconstruction of human metabolism. *Nat Biotechnol*. 2013;31(5):419–425.
14. Shimakata T, Mihara K, Sato R. Reconstitution of hepatic microsomal stearoyl-coenzyme A desaturase system from solubilized components. *J Biochem*. 1972;72(5):1163–1174.
15. Thiam AR, Farese RV, Walther TC. The biophysics and cell biology of lipid droplets. *Nat Rev Mol Cell Biol*. 2013;14(12):775–786.
16. Hirschey MD, et al. SIRT3 regulates mitochondrial fatty-acid oxidation by reversible enzyme deacetylation. *Nature*. 2010;464(7285):121–125.
17. Menendez JA, Lupu R. Fatty acid synthase and the lipogenic phenotype in cancer pathogenesis. *Nat Rev Cancer*. 2007;7(10):763–777.
18. Shackleton M, et al. Generation of a functional mammary gland from a single stem cell. *Nature*. 2006;439(7072):84–88.
19. Stingl J, et al. Purification and unique properties of mammary epithelial stem cells. *Nature*. 2006;439(7079):993–997.
20. Camarda R, et al. Inhibition of fatty acid oxidation as a therapy for MYC-overexpressing triple-negative breast cancer. *Nat Med*. 2016;22(4):427–432.
21. Meier-Abt F, et al. Parity induces differentiation and reduces Wnt/Notch signaling ratio and proliferation potential of basal stem/progenitor cells isolated from mouse mammary epithelium. *Breast Cancer Res*. 2013;15(2):R36.
22. Reuter S, Gupta SC, Chaturvedi MM, Aggarwal BB. Oxidative stress, inflammation, and cancer: how are they linked? *Free Radic Biol Med*. 2010;49(11):1603–1616.
23. Nakamura J, Swenberg JA. Endogenous apurinic/apyrimidinic sites in genomic DNA of mammalian tissues. *Cancer Res*. 1999;59(11):2522–2526.
24. Nakamura J, Walker VE, Upton PB, Chiang SY, Kow YW, Swenberg JA. Highly sensitive apurinic/apyrimidinic site assay can detect spontaneous and chemically induced depurination under physiological conditions. *Cancer Res*. 1998;58(2):222–225.
25. Joshi PA, et al. Progesterone induces adult mammary stem cell expansion. *Nature*. 2010;465(7299):803–807.
26. Reliene R, Fischer E, Schiestl RH. Effect of N-acetyl cysteine on oxidative DNA damage and the frequency of DNA deletions in atm-deficient mice. *Cancer Res*. 2004;64(15):5148–5153.
27. Poole AJ, Li Y, Kim Y, Lin SC, Lee WH, Lee EY. Prevention of Brca1-mediated mammary tumorigenesis in mice by a progesterone antagonist. *Science*. 2006;314(5804):1467–1470.
28. Chua AC, Hodson LJ, Moldenhauer LM, Robertson SA, Ingman WV. Dual roles for macrophages in ovarian cycle-associated development and remodelling of the mammary gland epithelium. *Development*. 2010;137(24):4229–4238.
29. Gampenrieder SP, Rinnerthaler G, Greil R. Neoadjuvant chemotherapy and targeted therapy in breast cancer: past, present, and future. *J Oncol*. 2013;2013:732047.
30. Gonzalez-Angulo AM, et al. Gene expression, molecular class changes, and pathway analysis after neoadjuvant systemic therapy for breast cancer. *Clin Cancer Res*. 2012;18(4):1109–1119.
31. Budczies J, et al. Remodeling of central metabolism in invasive breast cancer compared to normal breast tissue - a GC-TOFMS based metabolomics study. *BMC Genomics*. 2012;13:334.
32. Cairns RA, Harris IS, Mak TW. Regulation of cancer cell metabolism. *Nat Rev Cancer*. 2011;11(2):85–95.
33. Baenke F, Peck B, Miess H, Schulze A. Hooked on fat: the role of lipid synthesis in cancer metabolism and tumour development. *Dis Model Mech*. 2013;6(6):1353–1363.
34. Wang G, Zhang X, Lee JS, Wang X, Yang ZQ, Zhang K. Endoplasmic reticulum factor ERLIN2 regulates cytosolic lipid content in cancer cells. *Biochem J*. 2012;446(3):415–425.
35. Yoon S, et al. Up-regulation of acetyl-CoA carboxylase alpha and fatty acid synthase by human epidermal growth factor receptor 2 at the translational level in breast cancer cells. *J Biol Chem*. 2007;282(36):26122–26131.
36. Kreike B, et al. Gene expression profiles of primary breast carcinomas from patients at high risk for local recurrence after breast-conserving therapy. *Clin Cancer Res*. 2006;12(19):5705–5712.
37. Viale A, et al. Oncogene ablation-resistant pancreatic cancer cells depend on mitochondrial function. *Nature*. 2014;514(7524):628–632.
38. Borger J, Kemperman H, Hart A, Peterse H, van Dongen J, Bartelink H. Risk factors in breast-conservation therapy. *J Clin Oncol*. 1994;12(4):653–660.
39. Vrieling C, et al. Can patient-, treatment- and pathology-related characteristics explain the high local recurrence rate following breast-conserving therapy in young patients? *Eur J Cancer*. 2003;39(7):932–944.
40. Fahlén M, et al. Hormone replacement therapy after breast cancer: 10 year follow up of the Stockholm randomised trial. *Eur J Cancer*. 2013;49(1):52–59.
41. Holmberg L, Anderson H, HABITS steering data monitoring committees. HABITS (hormonal replacement therapy after breast cancer--is it safe?), a randomised comparison: trial stopped. *Lancet*. 2004;363(9407):453–455.
42. Kenemans P, et al. Safety and efficacy of tibolone in breast-cancer patients with vasomotor symptoms: a double-blind, randomised, non-inferiority trial. *Lancet Oncol*. 2009;10(2):135–146.
43. Chlebowski RT, et al. Influence of estrogen plus progestin on breast cancer and mammography in healthy postmenopausal women: the Women's Health Initiative Randomized Trial. *JAMA*. 2003;289(24):3243–3253.
44. Kelsey JL, Gammon MD, John EM. Reproductive factors and breast cancer. *Epidemiol Rev*. 1993;15(1):36–47.
45. Yasueda A, Urushima H, Ito T. Efficacy and interaction of antioxidant supplements as adjuvant therapy in cancer treatment: A systematic review. *Integr Cancer Ther*. 2016;15(1):17–39.
46. Greenlee H, et al. Prevalence and predictors of antioxidant supplement use during breast cancer treatment: the Long Island Breast Cancer Study Project. *Cancer*. 2009;115(14):3271–3282.
47. Greenlee H, et al. Antioxidant supplement use after breast cancer diagnosis and mortality in the Life After Cancer Epidemiology (LACE) cohort. *Cancer*. 2012;118(8):2048–2058.
48. Nechuta S, et al. Vitamin supplement use during breast cancer treatment and survival: a prospective cohort study. *Cancer Epidemiol Biomarkers Prev*. 2011;20(2):262–271.